Exploring the Dynamics of Wind Energy Harvesters: VIV Turbines and Piezoelectrics

Felipe Lima de Abreu[1], Clivaldo de Oliveira[1], Rodrigo B. Santos [1], Murilo Cesar Filipus[1], José Manoel Balthazar [2], Angelo M. Tusset [3], Marcus Varanis [4]

[1]*Faculty of Engineering, Federal University of Grande Dourados*
Rodovia Dourados-Itahum, Km 12 - Cidade Universitária, 79804-970, Dourados/MS, Brazil
felipeabreu507@gmail.com, clivaldooliveira@ufgd.edu.br, rodrigobsantos@ufgd.edu.br, murilocesarf77@gmail.com
[2]*Faculty of Engineering, São Paulo State University*
Av. Eng. Luís Edmundo Carrijo Coube, 2681 - Nucleo Res. Pres. Geisel, 17033-360, Bauru/SP, Brazil
jmbaltha@gmail.com
[3]*Federal University Technology of Paraná*
R. Doutor Washington Subtil Chueire, S/N - Jardim Carvalho, 84017-220, Ponta Grossa/PR, Brazil
a.m.tusset@gmail.com
[4]*Physics Institute, Federal University of Mato Grosso do Sul (UFMS).*
Av. Costa e Silva, s/nº - Bairro Universitário, 79070-900, Campo Grande/MS, Brazil
marcus.varanis@gmail.com

Abstract. Wind energy is recognized not only for its high generating capacity among renewable sources, but also for its growing popularity in recent years. However, conventional wind turbines, which rely on blades to capture wind energy, present significant challenges, including noise pollution, interference with bird migration and the frequent need for maintenance due to the complexity of their mechanical components. In an attempt to minimize these problems, current innovations include bladeless wind turbines (VBWT). These operate from wind-induced vibrations, mostly vortex-induced vibrations (VIV). Among the various designs that have been documented, those that exploit energy generation through electromagnetic induction and piezoelectric systems deserve to be highlighted, as they have gained increasing recognition in the academic sphere. In this context, this paper focuses on carrying out a dynamic analysis of a vortex-induced vibration energy harvester (VIVEH), which will have its energy generated from a piezoelectric patch connected to a beam with nonlinear stiffness due to a magnetic coupling. The system will have its equations of motion simulated using a Runge-Kutta integrator implemented in the Python programming language, where its responses will be analyzed in the time domain by studying the system's sensitivity to different wind speeds, and in the frequency domain using tools such as Fast Fourier Transforms (FFT) and Continuous Wavelet Transforms (CWT). The results focus on analyzing the influence of the beam's non-linearity and its response in the frequency and time domain for different wind speeds.

Keywords: Energy Haversting, VIV, Nonlinear Dynamics, Time Frequency Analysis

1 Introduction

Collecting data from sensors and the use of electricity is increasingly crucial, especially for devices operating in remote areas, which traditionally rely on chemical batteries or a complex infrastructure, leading to high costs and a significant environmental impact. To mitigate these challenges, part of the academic community has dedicated itself to developing embedded systems capable of self-energizing or supplying energy to other electronic devices, using energy harvesters (EH) that capture energy from the environment from various sources [1]. In particular, energy generated by wind and vibration has shown promise. For example, different types of wind turbines and piezoelectric generators are capable of converting air movement or mechanical vibrations into electricity, allowing the continuous operation of devices such as sensors or the powering of small electronics in a more sustainable way [2–4].

Within wind energy, there are several research projects that focus on obtaining energy from flow-induced vibration (FIV) phenomena. Among the EH that work from FIV, there are some classifications such as flutter, gallop and vortex-induced vibrations (VIV) [5]. The generation of energy by these phenomena occurs as follows:

flutter occurs when aerodynamic forces interact with a structure, leading to self-excited oscillations [6]. Gallop is a phenomenon in which a structure experiences oscillatory lateral movements due to transverse fluid flow [7]. And finally, VIVs arise when the passage of a fluid creates alternating vortices that exert periodic forces on a structure, resulting in vibrations that can be captured for energy generation [8].

The generation of energy from VIV has generated interest in different means of conversion, such as from electromagnetic interaction [9, 10] and through piezoelectric materials [11]. Due to their energy generation and easy implementation, piezoelectric transducers are the most widely used for this type of energy harvesting. A common method is to work with a piezoelectric beam and a cylindrical body, which operates in the lock-in region, which is when the natural frequency of the structure approaches the natural frequency of vortex shedding. Among this class of collectors, there is a bibliography that presents studies of different patterns on the surface of the body, as presented by [11], systems with multiple degrees of freedom [12] and advances in the area of nonlinear dynamics with energy collectors with nonlinear restoring force with the aim of increasing the synchronization region, as presented by [13, 14].

The model used in this article is the same one proposed in [14], which presents a nonlinear restoring force due to the implementation of an instability introduced by the addition of magnets to the common model. Thus, the aim of this work is to present the modeling of the energy collector, analyze the different solutions found and the lock-in regions, both in the time and frequency domains, using discrete Fourier transforms and continuous Wavelet transforms, as well as verifying the increase in the synchronization region.

2 Methodology

In this paper, the analysis will focus on the energy collector shown in Fig. 1(a), which consists of a cylinder supported by a beam that can oscillate. Energy is generated using a piezoelectric patch, which can convert vibrational energy into electrical energy, where the vibrational energy that will be converted will be the energy obtained from the aerodynamic phenomenon known as vortex-induced vibrations (VIV).

VIV is the phenomenon that occurs when a fluid flows around a cylindrical structure. When the fluid passes around the body, a cyclical vortex shedding is released, which acts as a force perpendicular to the direction of flow, causing the body to oscillate. The schematic presented has an instability created due to the implementation of magnets in the system, causing it to respond in a nonlinear way, as shown in [14].

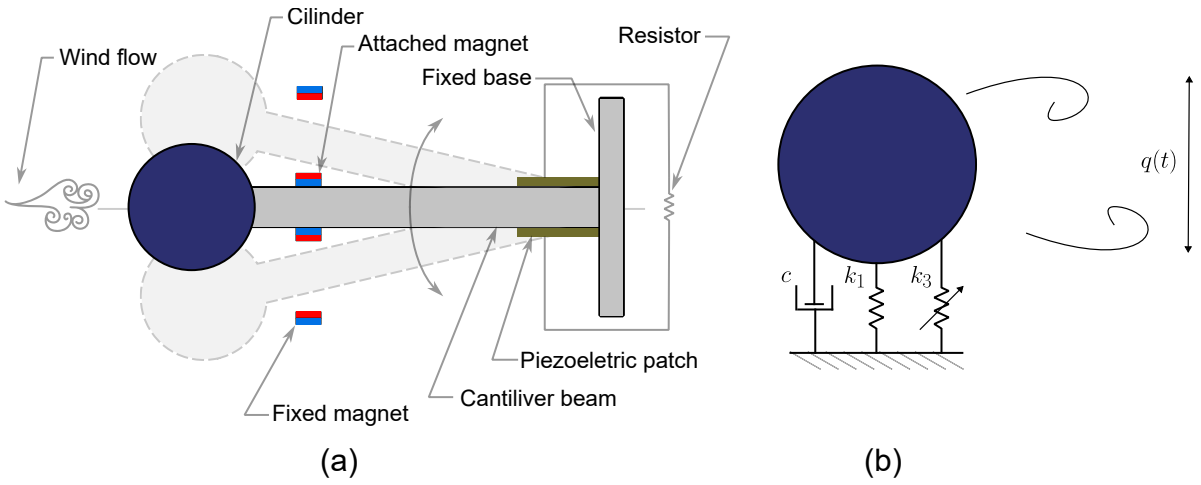

Figure 1. Illustrations (a) Energy harvester schematic, (b) Energy harvester model.

2.1 Model equations

In order to dynamically model vortex shedding, a commonly used approach is to use a modified Van der Pol model, where we will use the model suggested in [15], presented by eq. (1). Where q is the reduced vortex lift coefficient, the variation of the lift and drag coefficients is given by $C_l = 0.5q(t)C_{l0}$ and $C_d = \dot{x}(t)C_{d0}$, A and β are experimentally adjusted values and ω_{shed} is the vortex shedding frequency, given by $\omega_{shed} = 2\pi S_t U D^{-1}$ [13].

$$\ddot{q} + \beta\omega_{shed}(q^2 - 1)\dot{q} + \omega_{shed}^2 q = \frac{A}{D}\ddot{x} \tag{1}$$

Regarding the amplitude of the VIV force, this is given by eq. (2), which takes into account both the lift and drag forces. Where ρ is the density of the fluid in which the system is immersed, U is the velocity of the incoming flow, D the diameter of the cylinder and L the length of the cylinder.

$$F_{viv} = \frac{\rho U^2 DL}{2} C_l - \frac{\rho U DL}{2} C_d \tag{2}$$

Figure 1(b) shows the dynamic model of the mechanical part of the system. For this study, only the first vibration mode of the beam will be considered, thus assuming a spring-mass model, given by eq. (3). Where x will be the displacement of the tip of the beam, m the equivalent mass and c the viscous damping. The restoring force will be modeled from a polynomial function of the type $k_1 x + k_3 x^3$, to model the stiffness of the beam and the repulsion due to magnetic interaction.

$$m\ddot{x} + c\dot{x} + k_1 x + k_3 x^3 - \theta v = \frac{1}{2}\rho U^2 DL \frac{C_{l0}}{2} q - \frac{1}{2}\rho U DL C_{d0}\dot{x} \tag{3}$$

Finally, eq. (4) models the generation of energy from the piezoelectric adhesive. Where v will be the voltage generated, C_p the capacitance of the piezoelectric, R an external resistance and θ the conversion coefficient between electrical and mechanical energy.

$$C_p\dot{v} + \frac{v}{R} + \theta\dot{x} = 0 \tag{4}$$

2.2 Parameters

For this study, we will use the parameters of the same model presented in [13, 14], which are presented in Table 1.

Table 1. System parameters.

Parameters	Values	Units
Equivalent mass, m	0.0078	kg
Mechanical damping coefficient, c	0.003	Nsm^{-1}
Linear stiffness, k_1	26	N/m
External Resistance, R	10^6	Ω
Cylinder diameter, D	0.06	m
Electromechanical coupling coefficient, θ	$2 \cdot 10^5$	N/V
Length, L	0.09	m
Mean Steady Lift Coefficient, C_{l0}	0.3	-
Drag Coefficient, C_{d0}	1.2	-
Capacitance of the piezoelectric patch, C_p	100	nF
Experimental Constants, A and β	12, 0.24	-
Strouhal Number, S_t	0.2	-

The interaction presented by the nonlinear stiffness dynamics is given by the parameters shown in Fig. 2.

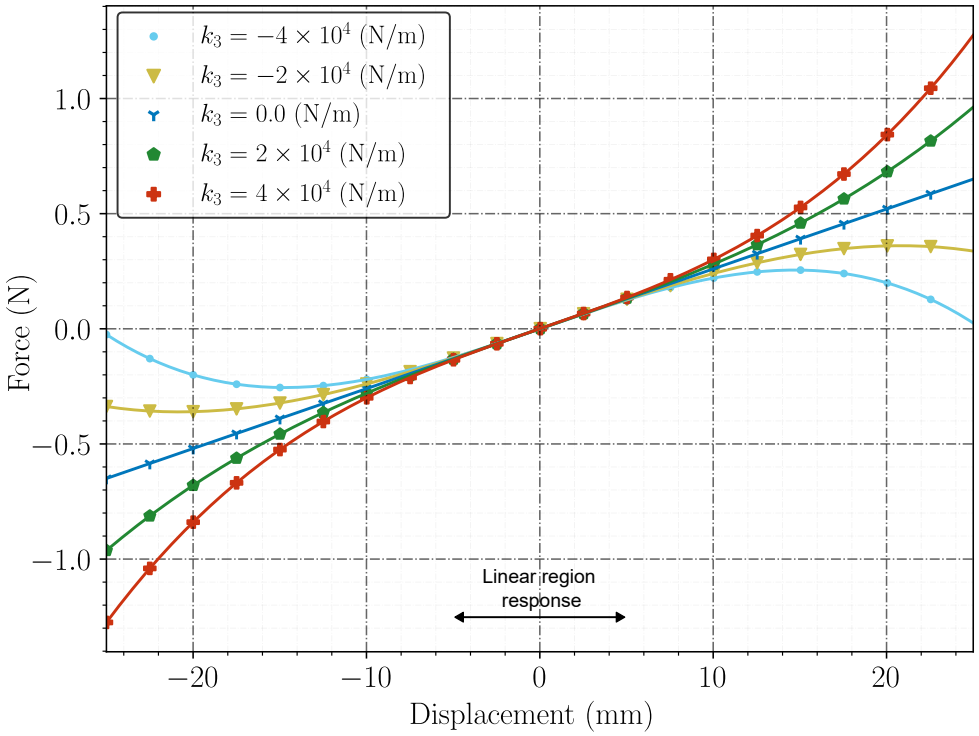

Figure 2. Force response for the stiffness considered.

3 Results

The results in this section were obtained using the parameters presented in the previous section, where the simulations were carried out using the Python programming language and its main scientific libraries. For the simulation, it was necessary to integrate eqs. (1, 3, 4). The system was integrated using a fourth-order Runge-Kutta integrator, with a simulation time of 50 s and a time step of $dt = 5 \times 10^{-4}$ s, which, after refining the mesh, proved to be a valid parameter for the simulations.

The analysis here will focus on comparing the two solutions presented by the system's nonlinear dynamics. As presented by [14], there are two periodic solutions for the system parameters, one with a large amplitude and the other small. In this case, the large-amplitude solution can be observed when we switch to the nonlinear regime of the restoring force and can be observed when we increase the initial displacement condition. Thus, the simulations here will all have zero initial conditions, except for the initial displacement x, which will take on the values: $x(0) = 0.01$ m for the case of small oscillations and $x(0) = 0.025$ m for the case of large oscillations.

Figure 3 shows the lock-in region for the different nonlinear stiffnesses. This analysis was carried out by simulating the system's response to the same initial conditions by varying the flow velocity and obtaining the maximum amplitude after 30 s for both the displacement x and the voltage v. The system's response shows that hard stiffness, i.e. a positive constant k_3, leads to an increase in the synchronization region and greater energy generation. Soft stiffness, on the other hand, causes both the amplitude and the lock-in region of the system to decrease.

It can also be seen how sensitive the system is to this initial condition, since in the case of large amplitudes, for the hard stiffnesses, there is a notable increase in both displacement and voltage generation, while for the soft stiffnesses no considerable increase is observed. The following analyses will therefore focus on the stiffness $k_3 = 4 \times 10^4$ (N/m), which has benefited most from the introduction of nonlinear dynamics.

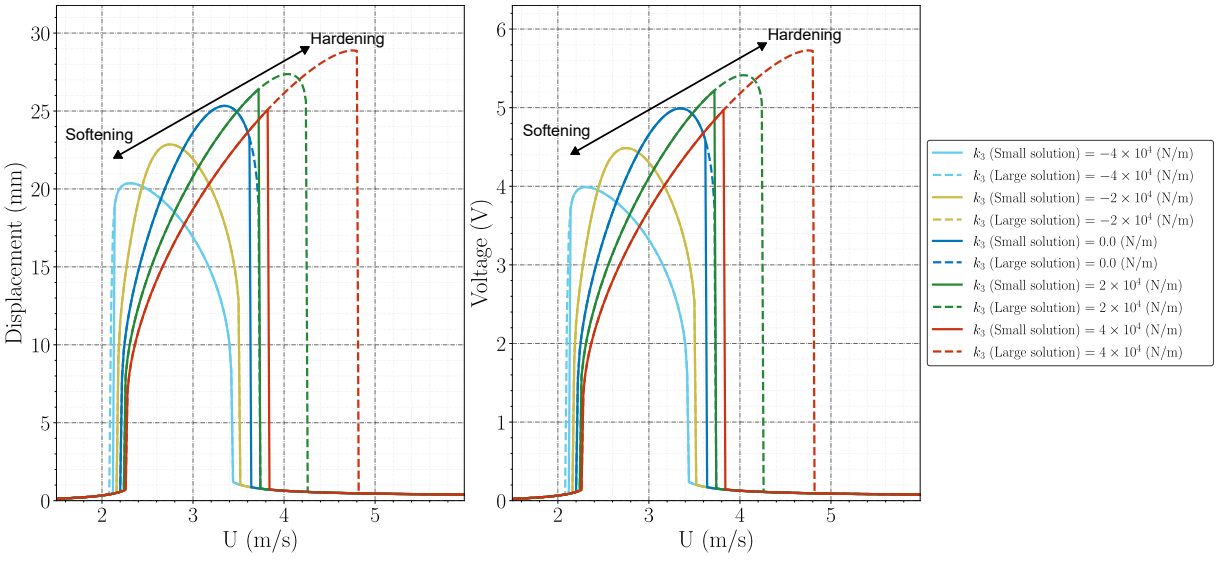

Figure 3. Frequency lock-in for the different springs stiffness (a) Displacement (b) Voltage.

The influence of these dynamics can be seen in the frequency domain response using discrete Fourier transforms. Figure 4 shows different Fourier transforms when varying the flow velocity for the stiffness $k_3 = 4 \times 10^4$ (N/m) for the case of small and large solutions, where the color map represents the voltage amplitude, with a red dotted line representing the frequency of vortex shedding.

In this analysis it is possible to see how the dynamics for the different initial conditions act in a similar way until the natural frequency of the system becomes lower than the vortex shedding frequency, where, for the case of small oscillations, there is a cut-off just after it becomes lower than the vortex shedding frequency, almost completely reducing energy generation. Unlike this case, for the large-amplitude solution, there is an increase in voltage generation and the lock-in region for higher wind speeds.

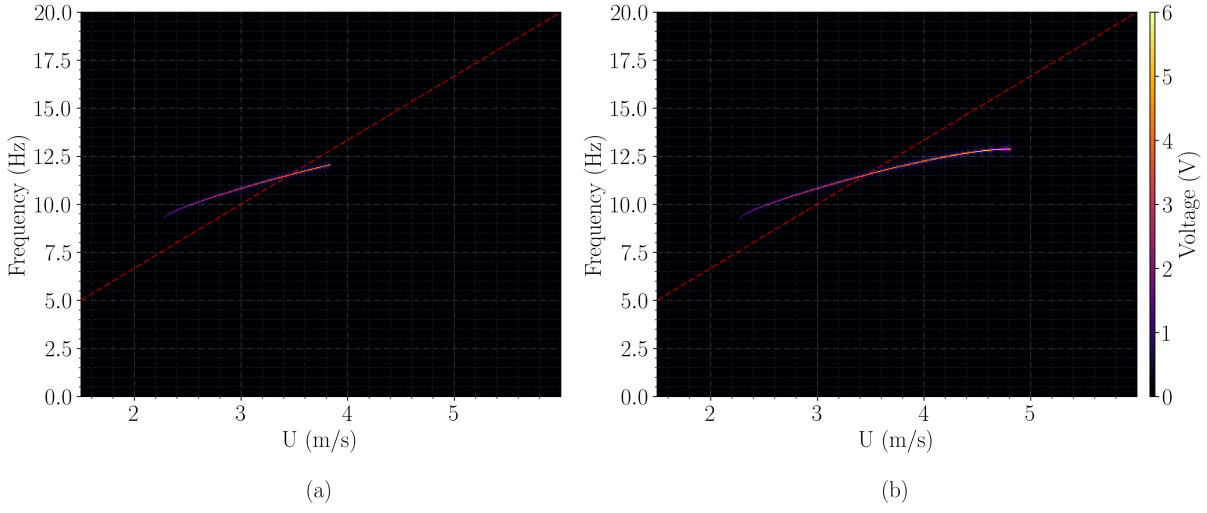

Figure 4. Discrete Fourier transform in the voltage signal for different wind velocities (a) Small solutions (b) Large solutions.

Focusing now on the lock-in response for the large solutions case, Fig. 5 is presented, which shows the time responses for the displacement, lift coefficient and voltage of the system for the two initial conditions with a flow velocity of $U = 4.8$ m/s. From this it can be seen that the behavior of both the displacement and the voltage are with low amplitudes for the case of small solutions, while for the case with large solutions there are the largest amplitudes in the flow velocity range. In this case, the drag coefficient varies linearly in the case of small solutions, and in a much more characteristic Van der Pol way in the case of large solutions.

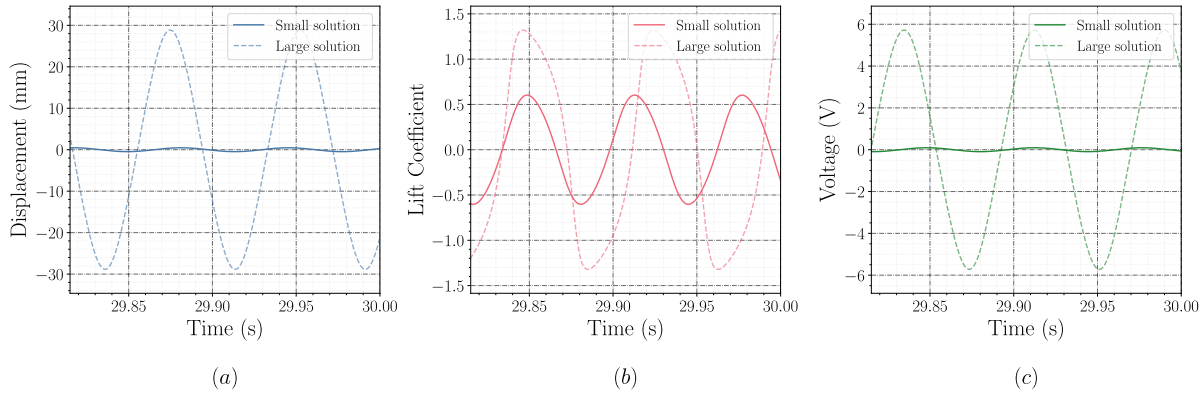

Figure 5. Time response (a) Displacement (b) Lift coefficient (c) Voltage.

When checking the instantaneous frequency over time, using a continuous Wavelet transform, shown in Fig. 6, it can be seen that for the two cases over the stationary period there are time invariant frequencies. In the case of small amplitudes there is a frequency of approximately 16 Hz, which is the vortex shedding frequency for this flow velocity, but in the case of large amplitudes there is a main frequency of around 12.7 Hz and a third order harmonic, showing that the nonlinear dynamics of the system generates large amplitude orbits when it has a minimum amount of initial energy.

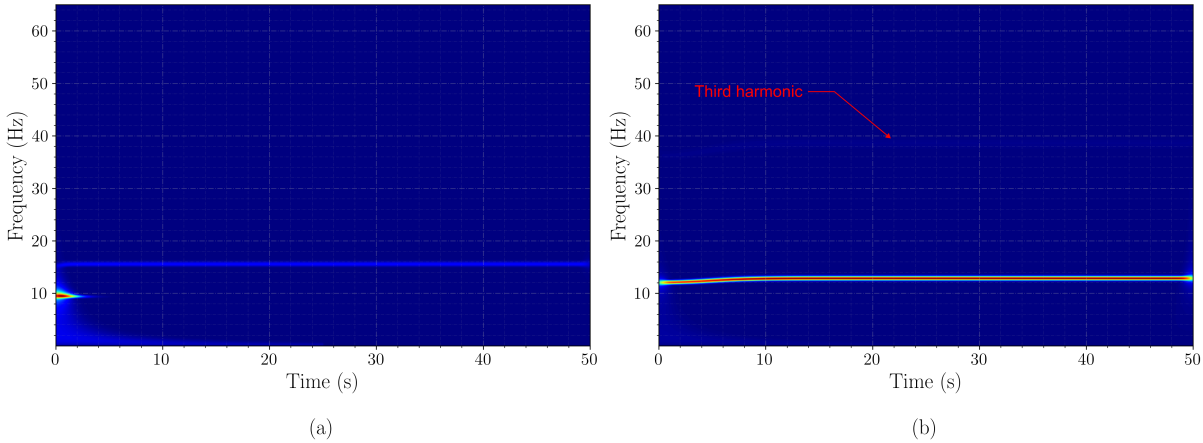

Figure 6. Continuous wavelet transform in the voltage signal (a) Small solutions (b) Large solutions.

4 Conclusions

This article presents an analysis of the dynamics of a nonlinear energy harvester excited by vortex-induced vibrations. The investigation is conducted by means of numerical simulations, which explore different solutions depending on the initial conditions. The results indicate that the introduction of a nonlinear restoring force causes a slight increase in the range of flow velocities corresponding to the lock-in region. However, when there is sufficient energy in the system, it is possible to observe solutions with large amplitudes, which result in a significant expansion of the lock-in region, particularly noticeable in the case of hard stiffness. This expansion of the lock-in region is also analyzed in the frequency domain, providing an additional perspective for studying the dynamics of the system.

Acknowledgements. The authors gratefully acknowledge the financial support from CNPq (National Council for Scientific and Technological) and the UFGD (Federal University of Grande Dourados).

Authorship statement. The authors hereby confirm that they are the sole liable persons responsible for the authorship of this work, and that all material that has been herein included as part of the present paper is either the property (and authorship) of the authors, or has the permission of the owners to be included here.

References

[1] M. R. Sarker, S. Julai, M. F. M. Sabri, S. M. Said, M. M. Islam, and M. Tahir. Review of piezoelectric energy harvesting system and application of optimization techniques to enhance the performance of the harvesting system. *Sensors and Actuators A: Physical*, vol. 300, pp. 111634, 2019.
[2] S. Roundy and P. K. Wright. A piezoelectric vibration based generator for wireless electronics. *Smart Materials and structures*, vol. 13, n. 5, pp. 1131, 2004.
[3] M. Gao, P. Wang, Y. Wang, and L. Yao. Self-powered zigbee wireless sensor nodes for railway condition monitoring. *IEEE Transactions on Intelligent Transportation Systems*, vol. 19, n. 3, pp. 900–909, 2017.
[4] M. M. A. Bhutta, N. Hayat, A. U. Farooq, Z. Ali, S. R. Jamil, and Z. Hussain. Vertical axis wind turbine–a review of various configurations and design techniques. *Renewable and Sustainable Energy Reviews*, vol. 16, n. 4, pp. 1926–1939, 2012.
[5] J. Wang, L. Geng, L. Ding, H. Zhu, and D. Yurchenko. The state-of-the-art review on energy harvesting from flow-induced vibrations. *Applied Energy*, vol. 267, pp. 114902, 2020.
[6] A. I. Aquino, J. K. Calautit, and B. R. Hughes. Integration of aero-elastic belt into the built environment for low-energy wind harnessing: Current status and a case study. *Energy Conversion and Management*, vol. 149, pp. 830–850, 2017.
[7] J. Sirohi and R. Mahadik. Harvesting wind energy using a galloping piezoelectric beam, 2012.
[8] A. B. Rostami and M. Armandei. Renewable energy harvesting by vortex-induced motions: Review and benchmarking of technologies. *Renewable and Sustainable Energy Reviews*, vol. 70, pp. 193–214, 2017.
[9] D. Y. Villarreal and V. B. SL. Viv resonant wind generators. *Vortex Bladeless SL*, 2018.
[10] I. Bahadur. Dynamic modeling and investigation of a tunable vortex bladeless wind turbine. *Energies*, vol. 15, n. 18, pp. 6773, 2022.
[11] J. Wang, S. Sun, L. Tang, G. Hu, and J. Liang. On the use of metasurface for vortex-induced vibration suppression or energy harvesting. *Energy conversion and management*, vol. 235, pp. 113991, 2021.
[12] D. Lu, Z. Li, G. Hu, B. Zhou, Y. Yang, and G. Zhang. Two-degree-of-freedom piezoelectric energy harvesting from vortex-induced vibration. *Micromachines*, vol. 13, n. 11, pp. 1936, 2022.
[13] X. Ma, Z. Li, H. Zhang, and S. Zhou. Dynamic modeling and analysis of a tristable vortex-induced vibration energy harvester. *Mechanical Systems and Signal Processing*, vol. 187, pp. 109924, 2023.
[14] Z. Li, H. Zhang, G. Litak, and S. Zhou. Periodic solutions and frequency lock-in of vortex-induced vibration energy harvesters with nonlinear stiffness. *Journal of Sound and Vibration*, vol. 568, pp. 117952, 2024.
[15] M. L. Facchinetti, E. De Langre, and F. Biolley. Coupling of structure and wake oscillators in vortex-induced vibrations. *Journal of Fluids and structures*, vol. 19, n. 2, pp. 123–140, 2004.